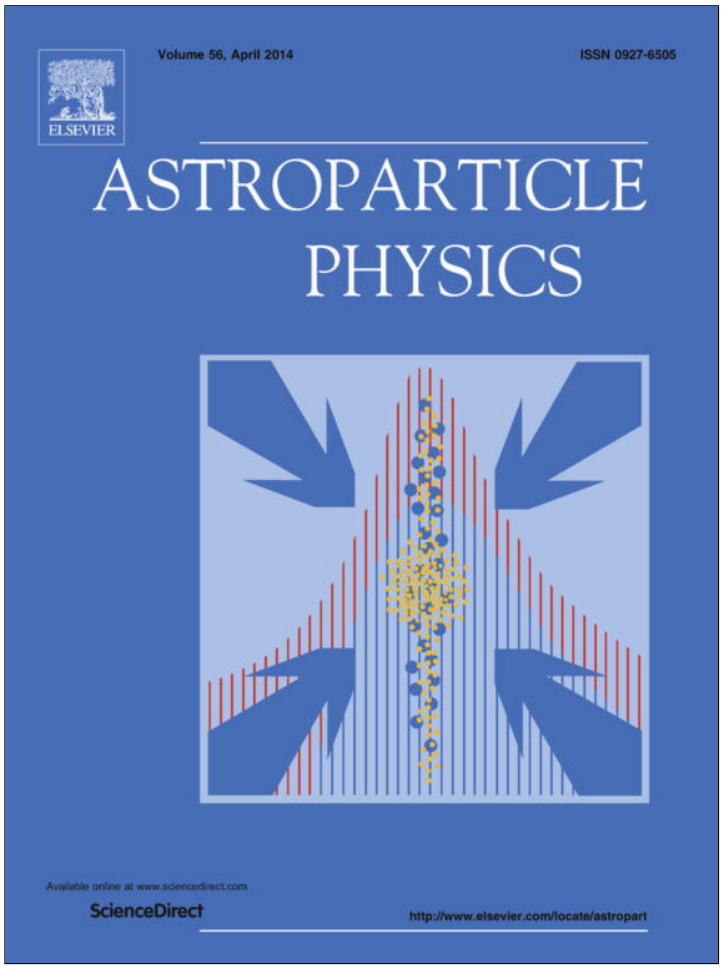

Astroparticle Physics 56 (2014) 9–15

Contents lists available at ScienceDirect

Astroparticle Physics

journal homepage: www.elsevier.com/locate/astropart

Astrophysical ZeV acceleration in the relativistic jet from an accreting supermassive blackhole ☆

Toshikazu Ebisuzaki [a,*], Toshiki Tajima [b]

[a] RIKEN, 2-1 Hirosawa, Wako 351-1198, Japan
[b] University of California, Irvine, CA 92679, United States

ARTICLE INFO

Article history:
Received 26 November 2013
Accepted 12 February 2014
Available online 20 February 2014

Keywords:
Acceleration of particles
Accretion
Accretion disks
Relativistic processes
Galaxies: jets
Galaxies: nuclei
Gamma rays: galaxies

ABSTRACT

An accreting supermassive blackhole, the central engine of active galactic nucleus (AGN), is capable of exciting extreme amplitude Alfven waves whose wavelength (wave packet) size is characterized by its clumpiness. The pondermotive force and wakefield are driven by these Alfven waves propagating in the AGN (blazar) jet, and accelerate protons/nuclei to extreme energies beyond Zetta-electron volt ($\mathrm{ZeV} = 10^{21}$ eV). Such acceleration is prompt, localized, and does not suffer from the multiple scattering/bending enveloped in the Fermi acceleration that causes excessive synchrotron radiation loss beyond 10^{19} eV. The production rate of ZeV cosmic rays is found to be consistent with the observed gamma-ray luminosity function of blazars and their time variabilities.

1. Introduction

The origin of ultra-high energy cosmic rays (UHECRs) with energies 10^{20} eV remains a puzzle of astrophysics. It is generally believed to be extragalactic ([1], references therein). The production of UHECRs has been discussed mainly in the framework of the Fermi acceleration [2], in which charged particles gain energy through a numerous number of scatterings by the magnetic clouds. One of the necessary conditions of Fermi acceleration is the magnetic confinement: the Hillas criterion sets a constraint on the product of the magnetic field strength B and extension R of the candidate objects (Hillas criterion) [3]: $W \leqslant W_{\max} \sim z(B/1\ \mu\mathrm{G})(R/1\ \mathrm{kpc})$ EeV, where z is the charge of the particle. The possible candidate objects (but only marginally satisfying the Hillas criterion for 10^{20} eV production) are neutron stars, active galactic nuclei (AGN), gamma-ray bursts (GRBs), and accretion shocks in the intergalactic space. However, the acceleration of 10^{20} eV particles even in those candidate objects is not easy for the Fermi mechanism because of (1) the large number of scatterings necessary to reach highest energies, (2) energy losses through the synchrotron emission at the bending associated with scatterings, and (3) difficulty in the escape of particles which are initially magnetically confined in the acceleration domain [1].

In the present paper we point out that there is an alternative way to accelerate charged particles (protons, ions, and electrons) to ultra-high energies in cosmic conditions, in particular in the conditions of AGN, through the electromagnetic (EM) wave-particle interaction. Along this path two conditions are necessary: (a) the accelerating structure (wave) should have a relativistic propagation velocity (phase velocity) very close to the speed of light c; (b) the wave should have a relativistic amplitude (i.e. so large an amplitude that the particle acquires relativistic momentum in one oscillation period of the wave, $e_jE/\omega > m_jc$, where E and ω are the wave electric field and frequency, e_j and m_j are the charge and mass of the jth particle). The condition (b) is needed because the electromagnetic field acceleration can yield acceleration in the direction of the wave propagation only from the nonlinear force of $v \times B/c$, called the ponderomotive force, and this term becomes significant only when the amplitude becomes relativistic [4]. We note that these two conditions may be fulfilled in a number of astrophysical settings (as well as in many modern terrestrial laboratories [5]). When the conditions (a) and (b) are fulfilled, this acceleration mechanism for UHECR generation has advantages over the Fermi mechanism, for the following reasons:

1. The ponderomotive field provides an extremely high accelerating field.

☆ We would like to dedicate this paper to the late Professor Yoshiyuki Takahashi, whose encouragement on this work has been crucial.

* Corresponding author. Tel.: +81 484679414.
E-mail address: ebisu@postman.riken.jp (T. Ebisuzaki).

http://dx.doi.org/10.1016/j.astropartphys.2014.02.004
0927-6505/

2. It does not require particle bending, which would cause severe synchrotron radiation losses in extreme energies.
3. The accelerating fields and particles move in the collinear direction at the same velocity, the speed of light, so that the acceleration has a built-in coherence called "relativistic coherence" [6]; in contrast, the Fermi acceleration mechanism, based on multiple scatterings, is intrinsically incoherent and stochastic.
4. No escape problem [1] exists. Particles can escape from the acceleration region since the accelerating fields naturally decay out.
5. Whenever and wherever intense electromagnetic waves (with sufficiently high frequencies) are excited, such waves tend to exhibit coherent dynamics (see later for details).

Takahashi et al. [7] and Chen et al. [8] demonstrated that intense Alfven waves produced by a collision of neutron stars can create wakefields to accelerate charged particles beyond 10^{20} eV. Although such a neutron star collision is believed to be related to short gamma-ray bursts [9], it is rather rare for two neutron stars to hit each other directly: It requires the same masses, otherwise the tidal field of the more massive star destroys the less massive one to form an accretion disk. Chang et al. [10] conducted a one-dimensional numerical simulation showing that whistler waves emitted from an AGN produce wakefields to accelerate UHECRs.

The accreting supermassive blackhole, the central engine of an AGN, is one of the candidates for wakefield acceleration. The accretion disk repeats transitions between a highly magnetized (low-beta) state and a weakly magnetized (high-beta) state [11]. In fact, O'Neil et al. [12] have found that magnetic transitions with 10–20 orbital periods are predominant in the inner disk through their 3D simulation. Strong pulses of Alfven waves excited in the accretion disk at the transition can create intense pondermotive potential in the relativistic jet launched from the innermost region of the accretion disk. Our analysis finds that this pondermotive force naturally accelerates protons and nuclei up to extreme energies of ZeV (10^{21} eV).

In the present paper, we carry out a quantitative evaluation of the system of an accreting blackhole which consists of the blackhole itself, an accretion disk, and relativistic jets (Fig. 1), to lead to the generation of UHECRs beyond 10^{20} eV. The paper is organized as follows: We introduce our model for the generation of the intense accelerating structure based on the Tajima-Dawson mechanism [4] that is not hampered by the Fermi mechanism limitations in Section 2, and find that the highest energy is achievable around an accreting blackhole (AGN) in Section 3. Astrophysical implications are discussed in Section 4.

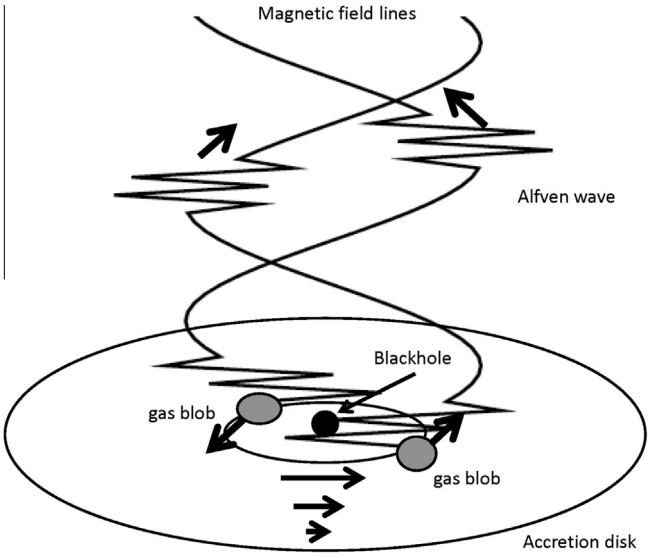

Fig. 1. Schematic diagram of the production of intensive Alfven waves in an accretion disk. A gas blob formed near the inner edge of the accretion disk severely shakes the magnetic fields and excites relativistic Alfven waves, which propagate along the magnetic field line of the jet.

2. Intense pondermotive mechanism

An accretion disk is formed around a blackhole when gas accretes onto it. Since the angular velocity is higher in inner orbits, there arises a strong shear flow between gases circulating at different radii in the disk. Since the gas is almost fully ionized and Ohmic loss is negligible, magnetic fields are stretched and amplified by the shear motion. The resultant toroidal magnetic field acts as an enhanced friction between gases circulating in the different orbits and transfers the angler momentum outward, while gas is pushed inward because of the reaction of the momentum exchange.

The inner edge of the accretion disk is located around $R = 3R_g$, where

$$R_g = 2GM/c^2 = 3.0 \times 10^{13}(m/10^8)\ \mathrm{cm} \tag{1}$$

is the gravitational radius of the blackhole. Here, m is the mass of the blackhole in the unit of solar mass (2.0×10^{33} g). An ergo-sphere appears just outside of the causality horizon of the blackhole. The gas inside the ergo-sphere and outside the horizon can extract rotational energy from the blackhole, if it is magnetized. This energy then drives relativistic jets in the two axial directions of the accretion disk [13]. The Lorentz factor Γ of the bulk motion of the jet is observed as $10 \sim 30$ in the case of active galactic nuclei.

According to Shibata et al. [11], the accretion disk makes transitions between two states: In the weakly magnetized state, magnetic fields are amplified by a strong shear flow, grow until at a certain point, and decay out; in other words, the disk makes transitions between these two states repeatedly. As a result, strong fluctuations are induced in the innermost region of the accretion region ($R < 10R_g$). The physical parameters in this innermost region ($R < 10R_g$) are estimated according to Shakura and Sunyaev [14]:

$$\varepsilon_D = 6.6 \times 10^6 (m/10^8)^{-1}\ \mathrm{erg\ cm^{-3}}, \tag{2}$$

$$n_D = 2.9 \times 10^{14} (\dot{m}/0.1)^{-2} (m/10^8)^{-1}\ \mathrm{cm^{-3}}, \tag{3}$$

$$Z_D = 2.2 \times 10^{13} (\dot{m}/0.1)(m/10^8)\ \mathrm{cm}, \tag{4}$$

$$B_D = 1.8 \times 10^3 (m/10^8)^{-1/2}\ \mathrm{G}, \tag{5}$$

where $\dot{m}$ is the accretion rate normalized to the critical accretion rate ($\dot{M}_c = L_{\mathrm{Edd}}/0.06c^2$) [14]. The viscosity parameter α is assumed to be 0.1 in the present paper. From the definition of m and $\dot{m}$, the total luminosity of the accreting blackhole is given by

$$L_{\mathrm{tot}} = 1.3 \times 10^{45} (\dot{m}/0.1)(m/10^8)\ \mathrm{erg\ s^{-1}}. \tag{6}$$

The wavelength λ_A of Alfven waves emitted from the accretion disk is calculated as [15]:

$$\lambda_A = (V_{AD}/C_{sD})(\Omega/A) Z_D = B_D Z_D / 3(4\pi\varepsilon_D)^{1/2} = 5.8 \times 10^{12} (\dot{m}/0.1)(m/10^8)\ \mathrm{cm}, \tag{7}$$

where V_{AD} is the Alfven velocity in the accretion disk, which is calculated as:

$$V_{AD} = B_D/\sqrt{4\pi m_H n_D} = 2.4 \times 10^7 (\dot{m}/0.1) \tag{8}$$

and C_{sD} is the sound velocity in the accretion disk:

$$C_{sD} = \sqrt{\varepsilon_D / m_H n_D}, \tag{9}$$

where m_H is the proton mass. We assume magnetic field in the accretion disk as B_D and the Keplarian rotation of gas inside the disk, i.e. $\Omega/A = 4/3$. The magnetic energy E_B stored in the innermost region of the accretion disk ($R < 10R_g$) is estimated as:

$$E_B = (B_D^2/4\pi)\pi(10R_g)^2 Z_D = 1.6\times10^{48}(\dot{m}/0.1)(m/10^8)^2 \text{ erg}. \quad (10)$$

The Alfven waves excited in the accretion disk propagate along the global magnetic field of the jet. The normalized vector potential a, which is the Lorentz-invariant strength parameter of the wave [5], is calculated as:

$$a = eE/m_e\omega_A c, \quad (11)$$

where m_e and e are the electron mass and charge, and we used $E = (V_{AD}/c)^{1/2}B_D$ and $\omega_A = 2\pi V_{AJ}/\lambda_A \simeq 2\pi c/\lambda_A$. The former comes from the conservation of Alfven energy flux, i.e., $\Phi_{AJ}(= cE\times B/4\pi) = \Phi_{AD}(= V_{AD}B_D^2/4\pi)$. We find that a is much greater than unity for a large class of AGN disks. We also find that the Alfven velocity in the jet (except at the very vicinity of the blackhole) is close to c, and thus these Alfven waves exert an intense pondermotive force on electrons and ions. In this $a \gg 1$ regime, the longitudinal pondermotive acceleration dominates the transverse acceleration. As we have mentioned in the introduction (page 3), the Tajima-Dawson acceleration [4] requires the conditions (a) and (b). Ashour-Abdalla et al. [16] studied this acceleration mechanism in the astrophysical context, where the condition (b) is overwhelmingly satisfied. It was found [16] that while the pondermotive force accelerates particles ahead of the EM pulse, it causes a density cavity in and behind the pulse (which is the cause of the trailing wakefields). In more recent works with conditions closer to the terrestrial acceleration experiments, Refs. [18–20,17] found qualitatively similar results to Ashour-Abdalla's, although details vary due to parameter differences. Mourou et al., in his review paper [21], called the EM pulse "relativistic" when $m_H/m_e > a > 1$, and "ultra-relativistic" when $a > m_H/m_e > 1$. No terrestrial experiments so far have been performed in the "ultra-relativistic" regime. Only a limited number of theoretical works have been devoted to this regime. Therefore, the details of the dynamics of this regime remain to be investigated in the future. Within 1D, Ashour-Abdalla et al. [16] find that the greater a is in the "ultra-relativistic" regime, the more that the charge separation force is dominated by the EM pondermotive force, although it is expected that this effect may be mitigated in 2–3D. Thus this regime should be dominated by pondermotive acceleration.

The Alfven flux inside of the jet is assumed to be inversely proportional to πb^2, and b to the square root of the distance $D : b = 10R_g(D/3R_g)^{1/2}$. This scaling is consistent with the VLBI observation of the jet of M87, the closest AGN [22]. In such a case, the value of a for the wave propagating in the jet is calculated as:

$$a(D) = a_0(D/3R_g)^{-1/2}, \quad (12)$$

where D is the distance from the black hole along the jet, and a_0 is the value of a at the disk inner edge ($D = 3R_g$), which is estimated as:

$$a_0 = 2.3\times10^{10}(\dot{m}/0.1)^{3/2}(m/10^8)^{1/2}. \quad (13)$$

The Lorentz factor γ of the quivering motion of particles in the wave is of the order of a, i.e., $\gamma \sim a$.

The Alfven pulse generation, its collinear propagation feature, and its pondermotive acceleration all lead to coherent dynamics. In other words, the phase between the specific wave and the particles to be accelerated are tightly locked because the phase velocity of these waves (including the Alfven pulse in the jet under consideration) is very close to the speed of light, and because of the longitudinal (i.e., the direction parallel to the propagation of the Alfven wave which propagates along the direction parallel to the magnetic fields embedded in the jet) nature of the pondermotive force. Further note that the acceleration dynamics in one dimension is robust because of the relativistic coherence [6]. The mechanism known as dephasing (along with the pump depletion) [4,5] determines the maximum energy gain as well as the spectrum [23,8] (see Fig. 2).

We focus on the wave modes propagating parallel to the jet magnetic field, since these modes are effective for the linear acceleration to highest energies. The angular frequency of the Alfven wave is:

$$\omega_A = 2\pi V_{AJ}/\lambda_A \cong 2\pi c/\lambda_A = 3.2\times10^{-2}(\dot{m}/0.1)^{-1}(m/10^8)^{-1} \text{ Hz}, \quad (14)$$

where $V_{AJ} = B_J/\sqrt{4\pi m_H n_J}$ is the Alfven velocity in the jet. If we assume the conservation of magnetic flux in the jet, then the magnetic field B_J in the jet is scaled as:

$$B_J = \phi B_D(b/10R_g)^{-2} = \phi B_D(D/3R_g)^{-1}; \quad (15)$$

the plasma density n_J in the jet is calculated through the kinetic luminosity L_J of the jet,

$$L_J = n_J m_H c^3\Gamma^2\pi b^2 = \xi L_{tot} \quad (16)$$

from which one infers that

$$n_J = 2.6\times10^3(\dot{m}/0.1)(m/10^8)^{-1}(\xi/10^{-2})(\Gamma/20)^{-2}(D/3R_g)^{-1} \text{ cm}^{-3}. \quad (17)$$

The effective plasma frequency ω'_p is calculated as

$$\omega'_p = (4\pi n_J e^2/m_e\gamma\,\Gamma^3)^{1/2} \quad (18)$$

$$= 2.1\times10^{-1}\quad(\Gamma/20)^{-5/2}(\xi/10^{-2})^{1/2}(\dot{m}/0.1)^{-1/4}(m/10^8)^{-3/4}\times(D/3R_g)^{-1/4}\quad \text{Hz}. \quad (19)$$

On the other hand, the effective cyclotron frequency ω'_c is derived as

$$\omega'_c = eB_J/m_e c\gamma = 2.3\times10^0(\phi/2.0)(\dot{m}/0.1)^{-3/2}(m/10^8)^{-1}(D/3R_g)^{-1/2} \text{ Hz}. \quad (20)$$

As an Alfven wave pulse propagates along the jet, the density and magnetic fields decrease, and accordingly the ratios ω'_p/ω_A and ω'_c/ω_A plummet, as seen in Fig. 3 (for the case of $\dot{m} = 0.1$, $m = 10^8$, $\gamma = 20$, and $\xi = 10^{-2}$). As ω'_p approaches ω_A, the whistler branch of the Alfven pulse turns into the electromagnetic wave [10] and starts to excite pondermotive and wakefield potentials. The distance D_1 at which $\omega'_p = \omega_A$ is calculated as:

$$D_1/3R_g = 1.7\times10^3(\Gamma/20)^{-10}(\xi/10^2)^2(\dot{m}/0.1)^3(m/10^8). \quad (21)$$

On the other hand, the distance D_2 at which $\omega'_c = \omega_A$ is calculated as:

$$D_2/3R_g = 5.1\times10^3(\dot{m}/0.1)^{-1}(\phi/2.0)^2, \quad (22)$$

independent to $\dot{m}$ nor m. As D increases, ω'_c approaches ω_A. In spite of the cyclotron resonance at ω'_c, most of the wave energy is likely to tunnel from the whistler branch to the upper branch beyond the right-hand cut-off frequency

$$\omega_c^{rh} = \left[(\omega_c'^2 + 4\omega_p'^2)^{1/2} + \omega'_c\right]/2, \quad (23)$$

which is located above the cyclotron resonance ω'_c in the case of the cold and linear limit [24]. In addition to the linear evanescent tunneling, the nonlinear nature of the EM waves [16]; $a \gg 1$) results in the resonance broadening and the nonlinear tunneling (Fig. 2).

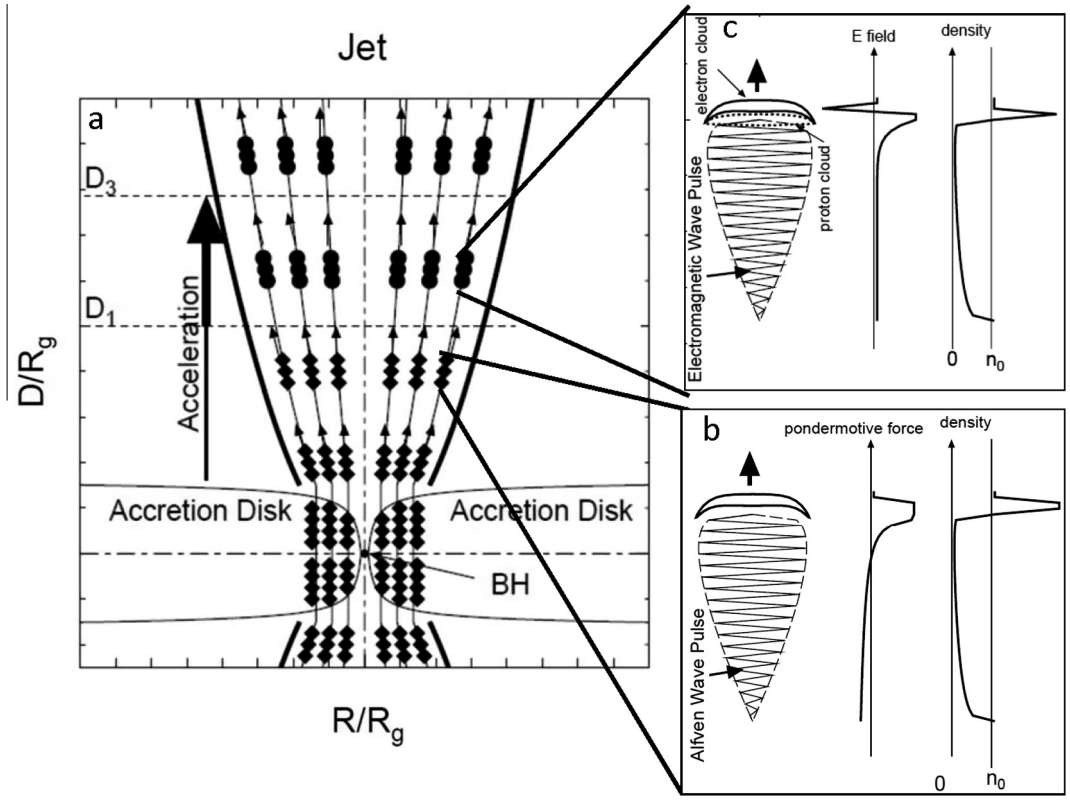

Fig. 2. (a) Schematic cross section of an disk/jet system around an accreting black hole (BH). Alfven waves (diamonds) are excited in the accretion disk and propagate along the magnetic field (thin solid curves) in the relativistic jet (thick solid curves). (b) In the pondermotive region ($\omega_c' > \omega_p' > \omega_A$), the pondermotive force of the intense Alfven wave pulse produces a bubble and accelerates particles. (c) The Alfven waves turn into electromagnetic waves (circles) as ω_A approaches and exceeds ω_p' and excites the accelerating structure whose pondermotive force fields accelerate charged particles longitudinally along the jet. We anticipate that in the extremely large a, the domain of wakefield acceleration is dwarfed by that of pondermotive acceleration in the 1D situation. In 2–3D, wakefield acceleration takes a greater role than in 1D.

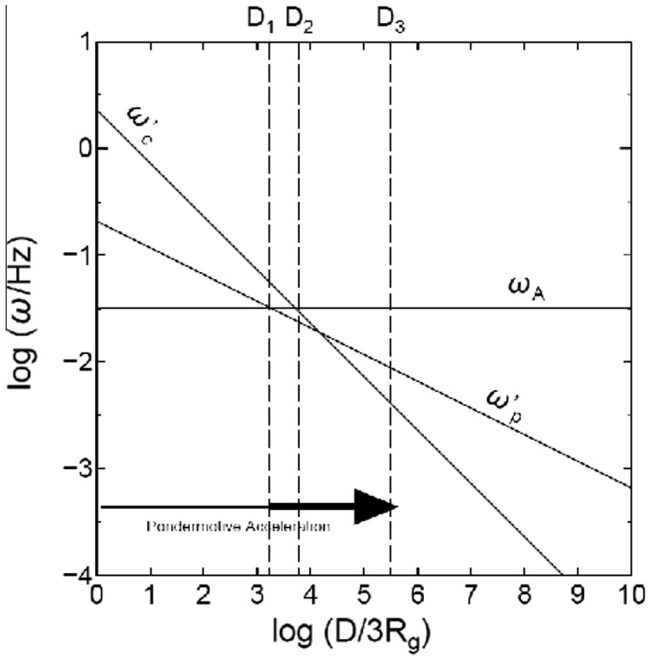

Fig. 3. Plasma frequency ω_p' and cyclotron frequency ω_c' are plotted against distance D along the jet for the case of $\dot{m} = 0.1$, $\xi = 10^{-2}$, $\Gamma = 20$, and $m = 10^8$. The pulse of Alfven waves with frequency ω_A is excited in the accretion disk ($D/R_g = 1$), propagating along the jet. Both ω_p' and ω_c' decrease as D increases. The Alfven wave (whistler branch) turns into an electromagnetic pulse around where $\omega_p' = \omega_A$, and drives the pondermotive potential to accelerate charged particles along the jet. Further mode-conversions are possible beyond $\omega_A > \omega_c'$. In this figure, we show the dominance of the pondermotive acceleration in the extreme regime of $a \gg 1$ in 1-D.

3. Highest energy cosmic rays

The phase velocity of Alfven wave in the jet is close to the light velocity because of the small n_J compared to n_D. In such a case, the particles are accelerated by the pondermotive force parallel to the direction of the propagation of the wave. The maximum energy W_{PM} in the observer's frame of the particles' gain in the region is calculated as:

$$W_{max} = z\int_0^{D_3} F_{pm}dD \tag{24}$$

$$= 4.6\times10^{19}\, z(\Gamma/20)(\dot{m}/0.1)^{1/2}(m/10^8)^{1/2}(D_3/3R_g)^{1/2}\ \text{eV}$$

$$= 2.9\times10^{22}\, z(\Gamma/20)(\dot{m}/0.1)^{4/3}(m/10^8)^{2/3}\ \text{eV}, \tag{25}$$

where

$$F_{pm} = \Gamma m_e c a \omega_A \tag{26}$$

is the pondermotive force of the wave. The acceleration length is assumed to be:

$$Z_{acc} = ca/\omega_A. \tag{27}$$

This is consistent with Ashour-Abdalla et al. [16]. Further, Barezhiani and Murushidze [25] obtained an exact nonlinear longitudinal plasma wave solution excited by a relativistic laser pulse, neglecting the quiver motion of protons.They found that the acceleration length is increased by a factor of a in a fashion similar to Eq. (27). This nature of acceleration lengthening can be expected to remain even in the case that proton quiver motion is not negligible, i.e., $a > 10^3$. They also found the plasma density is significantly reduced in the relativistic laser pulse because the plasma is evacuated by the

strong pondermotive force. Eq. 25 holds as far as Z_{acc} is greater than D. The distance D_3 is where the acceleration finishes, defined by the equation

$$D_3 = Z_{pd} = ac/\omega_A. \tag{28}$$

We find that particles arrive at D_1 before D_3, in other words:

$$D_3/3R_g = 3.9 \times 10^5 (\dot{m}/0.1)^{5/3} (m/10^8)^{1/3} > D_1/3R_g. \tag{29}$$

The energy spectrum of the accelerated charged particles has the power-law with the index of -2 in the 1-D model due to the multiple dephasing occurrences when particles ride on and off different peaks of the pondermotive or wakefield hills when the waves contain multiple frequencies (but with again the same phase velocity $\sim c$; [8]), i.e., $f(W) = A(W/W_{min})^{-2}$. As noted earlier, when the driving Alfven waves and their driven pondermotive fields hold a broad band of frequencies, their phase velocities and group velocities, respectively, are again close to the speed of light, providing the basis for the robust accelerating structure. When Alfven waves have two or three dimensional features, the dephasing is more prompt, leading to higher index of the spectrum (less than -2). Let κ be the energy conversion efficiency of the acceleration (including the mode convergence efficiency mentioned earlier), then $\kappa E_B = AW_{min}^2 ln(W_{max}/W_{min})$, i.e.

$$A = 1.6 \times 10^{33} \kappa \dot{m} m^2 [W_{min}^2 ln(W_{max}/W_{min})]^{-1}. \tag{30}$$

The recurrence rate ν_A of the Alfven pulse burst is evaluated as:

$$\nu_A = \eta V_{AD}/Z_D = 1.0 \times 10^2 \eta m^{-1} \text{ Hz}, \tag{31}$$

where η is episode-dependent, and on the order of unity. This is consistent with the 3-dimensional simulations conducted by O'Neill [12]. They found magnetic fluctuations, called Long Period Quasi Periodic Oscillations (LPQPO) with the period 10–20 times the Kepler rotation period. The luminosity L_{UHECR} of ultra-high energy cosmic rays is:

$$L_{UHECR} \sim \kappa \zeta E_B \nu_A = 1.6 \times 10^{33} (\kappa\zeta/0.01) \eta \dot{m} m \text{ erg s}^{-1}, \tag{32}$$

where $\zeta = ln(W_{max}/10^{20} \text{ eV})/ln(W_{max}/W_{min})$.

The pondermotive fields in the jets accelerate both ions and electrons and therefore the AGN jet is likely to be a strong gamma-ray source as well. Although the radiation loss of protons and nuclei is negligible as far as they are accelerated parallel to the magnetic field [26], that of electrons is likely to be significant, when electrons encounter magnetic fluctuations. The gamma-ray luminosity is, therefore, found to be as:

$$L_\gamma \sim \kappa E_B \nu_A = 1.6 \times 10^{34} (\kappa/0.1) \eta \dot{m} m \text{ erg s}^{-1}. \tag{33}$$

We summarize the major features of pondermotive/wakefield acceleration in an accreting supermassive blackhole in Table 1 (Fig. 4).

Table 1
Major features of pondermotive acceleration in an accreting supermassive blackhole.

	Values	Units
$2\pi/\omega_A$	$2.0 \times 10^2 (\dot{m}/0.1)(m/10^8)$	s
$1/\nu_A$	$1.0 \times 10^6 \eta^{-1} (m/10^8)$	s
D_3/c	$1.2 \times 10^9 (\dot{m}/0.1)^{5/3} (m/10^8)^{4/3}$	s
W_{max}	$2.9 \times 10^{22} z(\Gamma/20)(\dot{m}/0.1)^{4/3} (m/10^8)^{2/3}$	eV
L_{tot}	$1.2 \times 10^{45} (\dot{m}/0.1)(m/10^8)$	erg s^{-1}
L_A	$1.2 \times 10^{42} \eta (\dot{m}/0.1)(m/10^8)$	erg s^{-1}
L_γ	$1.2 \times 10^{41} (\eta\kappa/0.1)(\dot{m}/0.1)(m/10^8)$	erg s^{-1}
L_{UHECR}	$1.2 \times 10^{40} (\eta\kappa\zeta/10^{-2})(\dot{m}/0.1)(m/10^8)$	erg s^{-1}
L_{UHECR}/L_{tot}	$1.0 \times 10^{-5} (\eta\kappa\zeta/10^{-2})$	–
L_{UHECR}/L_γ	$1.0 \times 10^{-1} (\zeta/0.1)$	–

$\xi = L_J/L_{tot}$, $\eta = \nu_A Z_D/V_A$, $\kappa = E_{CR}/E_A$, and $\zeta = ln(W_{max}/(10^{20} eV))/ln(W_{max}/W_{min})$.

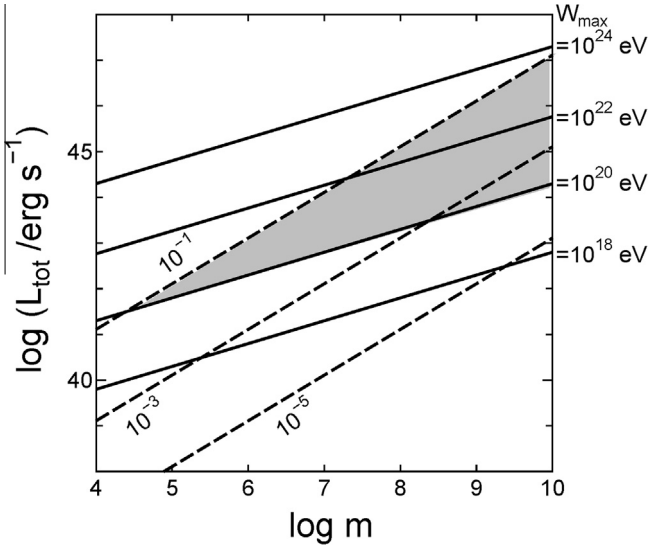

Fig. 4. The total luminosities of accreting blackholes are plotted against the blackhole mass (in the unit of solar mass) for various maximum attainable energy W_{max} (solid lines) for the case of $\Gamma = 20$ and $\xi = 10^{-2}$. Dashed lines are drawn for the values $\dot{m} = 10^{-5}$, 10^{-3}, and 10^{-1}. The grey triangle represents the parameter sets which allow the acceleration of UHECRs ($\geqslant 10^{20}$ eV). We set the upper limit of $\dot{m}$ to be around 0.1 for the pondermotive/wakefield acceleration to work, since the accretion disk becomes radiation dominant as $\dot{m}$ approaches unity, and the Alfven wave pulse becomes weaker than the estimate in the present paper.

4. Astrophysical implications and blazar characteristics

Radio galaxies belong to one category of AGN, which has radio lobes connected to the nucleus by relativistic jets. Their central engines are accreting supermassive ($m = 10^6 - 10^{10}$) blackholes. Urry and Padovani [27] pointed out that there are parent (or misaligned) populations of blazars, which show rapid time variations in many observational bands across radio to gamma rays (10 GeV) with distinct optical and radio polarizations because of their relativistic jet pointing almost toward us. The recent observation by the Fermi satellite reveals that many blazars emit strong gamma-rays in the GeV energy range [28–30].

We find that radio galaxies are most likely to be sources of UHECRs and their features fit well with the present theory of based on the Tajima-Dawson acceleration. First, according to Ajelloet et al. [31] and Broderick [32], the local gamma-ray luminosity density of blazars is estimated as 10^{37-38} erg s^{-1} (Mpc)$^{-3}$, taking into account the beaming effect of the relativistic jet. Assuming $L_{UHECR}/L_\gamma \sim \zeta \sim 0.1$ (see Table 1), our theoretical estimate of UHECR particle flux, averaged over the sky, becomes:

$$\overline{\Phi_{UHECR}} = 7.6 \times 10^{-2} l_{\gamma 37} (\zeta/0.1) \times (\tau_8/1.5) \text{ particles}/(100 \text{ km}^2 \text{ yr sr}). \tag{34}$$

Eq. (34) is consistent with observed flux of UHECR. Here, $l_{\gamma 37}$ is the local gamma-ray luminosity density of blazars (in the unit of 10^{37}erg s^{-1} (Mpc)$^{-3}$) and τ_8 is the life time of UHECR particles (in the unit of 10^8yr), which is determined by GZK process: Greisen[33] and Zatsepin and Kuzmin [34] predicted that cosmic-ray spectrum has a theoretical upper limit around 5×10^{19} eV, because of the opening of the channel to produce Δ^+ particles, which decay into pions (π^0 and $\pi^\pm$) and further into photons, electrons, protons, neutrons, and neutrinos. The flux of the cosmogenic neutrinos, produced by the GZK process, is as high as

$$\overline{\Phi_{UHEv}} = 5.4 \times 10^{-1} l_{\gamma 37} (\zeta/0.1) \times (\tau/100) \text{ particles}/(100 \text{ km}^2 \text{ yr sr}) \tag{35}$$

assuming the conversion efficiency of UHECR to UHEν to be 10%. This is consistent with the previous works for the case of $W_{\max} = 10^{21.5}$ (e.g. [35]). The recently observed PeV neutrinos with Ice Cube experiment [36] is also consistent if we assume the power law spectrum of the index of -2.2 in the energy region from PeV to ZeV. This level of UHEν flux may be detected by a next generation space borne detector of UHECR, like JEM-EUSO, which can achieve an integrated exposure of 10^6 km^2 str yr [37–40] as well as next generation neutrino facilities in the Antarctica, such as ANITA [41], ARA [42], and ARIANNA [43].

Second, blazars are also known for being highly variable at all wavelengths and all time scales. In the most extreme cases, the timescales of gamma-ray variability can be as short as a few minutes at very high energies ($\sim$ 100 GeV; VHE). Such variability has been detected in several BL Lacertae objects [36,44,45,29,46,47]. On the other hand, our pondermotive acceleration mechanism predicts the rapid time variability with all the time scales from the Alfven frequency ($2\pi/\omega_A \sim 100$ s), through the repetition period of the pulses ($1/\nu_A \sim$ days), and to the propagation time in the jet ($D_2/c, 1 \sim 10^2$ years). This time variability is both for ion acceleration variability for UHECRs as well as electron variability as observed in gamma rays (electron energies are limited by the radiation energy loss by PeV [48]. The finer structure of time variability is anticipated from our mechanism, as the magnetic structure may contain finer structure of braiding within the above quoted Alfven pulse. These observed blazer variabilities are the natural consequences deeply embedded in our model. Further, the coincidence of the pronounced luminosity peak and the reduced spectrum index observed by the Fermi satellite [49] for BL Lacs has so far no known explanation, but it is consistent with our theory.

Third, the multiple epoch observation of VLBA provides strong evidence that gamma-ray emission comes from a parsec scale jet [50–52]. Since the life time of high energy electrons is much shorter than the propagation time, they must be locally accelerated. This is consistent with the picture of the pondermotive acceleration, since a swarm of the electrons is accelerated locally in the pondermotive propagating in the jets. They are likely to emit a highly variable and polarized gamma-rays due to their high gamma-factor (see Fig. 4).

Our calculation yields the UHECR flux of gamma-ray emitting galaxies as:

$$\Phi_{\rm UHECR} = 3.5\times10^{-3}(\zeta/0.1)(\Phi_\gamma/10^{-10}\ \text{photons cm}^{-2}\ \text{s}^{-1}) \times (\overline{E_\gamma}/1\ \text{GeV})\ \text{particles}/(100\ \text{km}^2\ \text{yr}), \quad (36)$$

if the radiation pattern of UHECRs is the same as that of gamma-rays. Here, Φ_γ is the gamma-ray flux and $\overline{E_\gamma}$ is the average gamma-ray energy. We found nine gamma-ray emitting AGNs [30] within the GZK horizon ($\leqslant$ 70 Mpc; Table 2). The spectral indices are in the range of $-2 \sim -2.8$, which are consistent with our theory. Fig. 5 shows the distribution of the these gamma-ray emitting AGNs

Table 2
Nearby gamma-ray emitting AGNs detected by Fermi satellite [30].

Counterpart	lII	bII	Redshift	Flux (1–100 GeV) 10^{-10} erg cm^{-2}	Spectral index
NGC 0253	97.39	−87.97	0.001	6.2 ± 1.2	2.313
NGC 1068	172.10	−51.04	0.00419	5.1 ± 1.1	2.146
For A	240.15	−56.70	0.005	5.3 ± 1.2	2.158
M82	141.41	40.56	0.001236	10.2 ± 1.3	2.280
M87	283.78	74.48	0.0036	17.3 ± 1.8	2.174
Cen A Core	309.51	19.41	0.00183	30.3 ± 2.4	2.763
NGC 4945	305.27	13.33	0.002	7.5 ± 1.7	2.103
Cen B	209.72	1.72	0.012916	18.6 ± 3.5	2.325
NGC 6814	29.35	−16.02	0.0052	6.8 ± 1.6	2.544

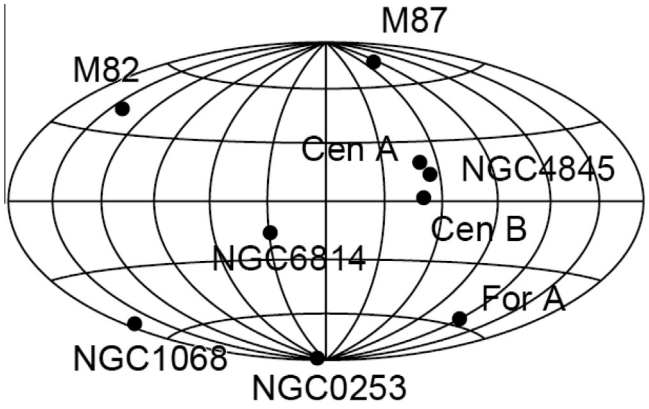

Fig. 5. Distribution of the nine gamma-ray emitting AGNs [30] in the sky.

in the sky. This flux value is large enough to allow identification of individual sources via a clustering of events in the JEM-EUSO detector, as well as by Takahashi et al. [37], Kajino et al. [38], Santangelo [39] and Gorodetzky et al. [40].

5. Conclusions

We have introduced the pondermotive acceleration mechanism arising from the Alfvenic pulse incurred by an accretion disk around a supermassive blackhole, the central engine of an AGN. This provides a natural account for UHECRs, and also for accompanying gamma-rays and their related observational characteristics, such as their luminosities, time variations, and structures. The severe physical constraints in the extreme ZeV energies by the Fermi acceleration have been lifted by the present mechanism. We have identified a number of areas of future research in need of further studies, including the cavity dynamics of super-intense Alfven pulses in 1–3 dimensions. We have presented a number of emerging astrophysical phenomena that are not easy to explain by existing theories, but are in line with natural consequences of the present acceleration mechanism.

Acknowledgments

We appreciate discussions with Profs. K. Abazajian, S.W. Barwick, S. Nagataki, A. Mizuta, and G. Yodh. The work was supported by the Norman Rostoker Fund at UCI.

References

[1] K. Kotera, A. Olinto, Ann. Rev. Astron. Astrophys. 49 (2011) 119.
[2] E. Fermi, ApJ 119 (1954) 1.
[3] A.M. Hillas, Ann. Rev. Astron. Astrophys. 22 (1984) 425.
[4] T. Tajima, J.M. Dawson, Phys. Rev. Lett. 43 (1979) 267.
[5] E. Esarey, C.B. Schroeder, W.P. Leemans, Rev. Mod. Phys. 81 (2009) 1229.
[6] T. Tajima, Proc. Jpn. Acad. Sci. B86 (2010) 147.
[7] Y. Takahashi, T. Tajima, L. Hillman, in: T. Tajima, K. Mima, H. Baldis (Eds.), High Field Science, Klewer, 2000, p. 171.
[8] P.C. Chen, T. Tajima, Y. Takahashi, Phys. Rev. Lett. 89 (2002) 161101.
[9] E. Nakar, Phys. Rep. 442 (2007) 166.
[10] F.Y. Chang et al., Phys. Rev. Lett. 102 (2009) 111101.
[11] K. Shibata, T. Tajima, R. Matsumoto, ApJ 350 (1990) 295.
[12] S.M. O'Neill et al., ApJ 736 (2011) 107.
[13] R.D. Blandford, R.L. Znajek, MNRAS 179 (1977) 433.
[14] N.I. Shakura, R.A. Sunyaev, Aap 24 (1973) 337.
[15] R. Matsumoto, T. Tajima, ApJ 445 (1995) 767.
[16] M. Ashour-Abdalla, J.N. Lebouf, T. Tajima, J.M. Dawson, C.F. Kennel, Phys. Rev. A 23 (1981) 1906.
[17] S.V. Bulanov, T. Esirkepov, M. Kando, N. Pirozhkov, Phys. Usp. 56 (2013) 429.
[18] T. Esirekepov, M. Borghesi, S. Bulanov, G. Mourou, T. Tajima, Phys. Rev. Lett. 92 (2004) 175003.
[19] T. Esirekepov, Y. Kato, S. Bulanov, Phys. Rev. Lett. 101 (2008) 265001.
[20] A.S. Pirozhkov et al., Phys. Rev. Lett. 108 (2012) 135004.

[21] G.A. Mourou, T. Tajima, S. Bulanov, Rev. Mod. Phys. 78 (2006) 309–371.
[22] K. Asada, M. Nakamura, ApJL 745 (2012) L28.
[23] K. Mima, W. Horton, T. Tajima, A. Hasegawa, in: Y. Ichikawa, T. Tajima (Eds.), Nonlinear Dynamics and Particle Acceleration, AIP, NY, 1991, p. 27.
[24] S. Ichimaru, Basic Principle of Plasma Physics , Benjamin, Reading, 1973 (p. 89).
[25] V.I. Berezhiani, I.G. Murusidze, Phys. Lett. 148 (1990) 338–340.
[26] J.D. Jackson, Classical Electrodynamics, John Wiley and Son, 1963.
[27] C.M. Urry, P. Padovani, ApJ 371 (1991) 60.
[28] R.C. Hartman, D.L. Bertsch, S.D. Bloom, et al., ApJ 123 (1999) 79.
[29] F. Aharonian, A.G. Akhperjanian, A.R. Bazer-Bachi, et al., ApJL 664 (2007) L71.
[30] M. Ackermann, M. Ajello, A. Allafort, et al., ApJ 743 (2011) 171.
[31] M. Ajello et al., ApJ 751 (2012) 108.
[32] A.E. Broderick, ApJ 752 (2012) 22.
[33] K. Greisen, Phys. Rev. Lett. 16 (1966) 748.
[34] G.T. Zatsepin, V.A. Kuzmin, JETP Lett. 4 (1966) 78.
[35] K. Kotera, D. Allard, A. Olinto, J. Cosmol. Astropart. Phys. 10 (2010) 013.
[36] T. Arlen et al., ApJ 762 (2013) 92.
[37] Y. Takahashi et al., New J. Phys. 11 (2008) 065009.
[38] F. Kajino et al., Nucl. Instrum. Methods 1 (2009) 422.
[39] A. Santangelo, Prog. Part. Nucl. Phys. 64 (2010) 366.
[40] P. Gorodetzky et al., Nucl. Instrm. Methods Phys. Res. Sec. A 626 (2011) S40.
[41] S.W. Barwick et al., Phys. Rev. Lett. 96 (2006) 171101.
[42] P. Allison, et al., 2011. Available from: <arXiv:1105.2854>.
[43] S.W. Barwick et al., in: 33rd International Cosmic Ray Conference, Rio De Janeiro, The Astroparticle Physics Conference, 2013.
[44] J.A. Gaidos, C.W. Akerlof, S. Biller, et al., Nature 383 (1996) 319.
[45] J. Albert, E. Aliu, H. Anderhub, et al., ApJL 666 (2007) L17.
[46] J. Aleksic, L.A. Antonelli, P. Antoranz, et al., ApJ 730 (2011) 8.
[47] S. Saito et al., ApJL 766 (2013) L11.
[48] A. Deng et al., Phys. Rev. STAB 15 (2012) 081303.
[49] A.A. Abdo et al., ApJ 710 (2010) 1271.
[50] M.L. Lister et al., AJ 137 (2009) 3718.
[51] A.P. Marscher, S.G. Jorstad, ApJ 710 (2010) L126.
[52] M. Lyutikov, M. Lister, ApJ 722 (2010) 197.